DOI: 10.1002/ejic.200900758

Pyrazine-Assisted Dimerization of Molybdenum(V): Synthesis and Structural Characterization of Novel Dinuclear and Tetranuclear Complexes

Barbara Modec,*[a] Martin Šala,[a] and Rodolphe Clérac[b,c]

Keywords: Molybdenum / Polynuclear complexes / Molecular building units / N ligands / Magnetic properties

Reactions of pyrazine (Pyz = $C_4H_4N_2$) with $[MoOCl_4(H_2O)]^-$ or $[MoOBr_4]^-$ afforded a series of complexes, dinuclear $[(MoOX_4)_2(Pyz)]^{2-}$ (X = Cl, Br), $[\{MoOCl_3(Pyz)\}_2O]^{2-}$ and tetranuclear $[(Mo_2O_4Cl_4)_2(Pyz)_2]^{4-}$ anions, with N-donor ligands engaged either in monodentate or bidentate bridging coordination. A dinuclear $[(MoOX_4)_2(Pyz)]^{2-}$ ion, which may be viewed as a linkage of two mononuclear subunits with a bidentate pyrazine, crystallizes either as a PyH^+ (pyridinium cation, $C_5H_5NH^+$; compound **1**), a $\{(C_2H_5)_4N\}^+$ (compound **2**) or a $\{(C_6H_5)_4P\}^+$ salt (compounds **3** and **4**). In $(PyH)_2[\{MoOCl_3(Pyz)\}_2O]$ (**5**) with an *anti*-$\{Mo_2O_3\}^{4+}$ core, pyrazine is bound to the metal through only one nitrogen atom. The tetranuclear $[(Mo_2O_4Cl_4)_2(Pyz)_2]^{4-}$ ion, a linkage of two metal–metal bonded $\{Mo_2O_4\}^{2+}$ cores with a pair of bidentate pyrazines, is found in two compounds, $(MeNC_5H_5)_2(PyzH_2)[(Mo_2O_4Cl_4)_2(Pyz)_2]$ (**6**) [$MeNC_5H_5^+$ = *N*-methylpyridinium cation, $PyzH_2^{2+}$ = pyrazinium(2+) cation] and $(PyH)_4[(Mo_2O_4Cl_4)_2(Pyz)_2]\cdot 2CH_3CN$ (**7**). In the presence of methanol, dinuclear $\{(C_6H_5)_4P\}_2[(MoOBr_4)_2(Pyz)]\cdot 2CH_3CN$ (**4**) was transformed directly into tetranuclear $(PyH)_4[(Mo_2O_4Br_4)_2(Pyz)_2]\cdot 2CH_3CN$ (**8**). All compounds were fully characterized by X-ray crystallography and IR spectroscopy. The compounds containing the $[(MoOX_4)_2(Pyz)]^{2-}$ ions display an irreversible electrochemical reduction behaviour. Temperature-dependent magnetic measurements on $\{(C_6H_5)_4P\}_2[(MoOX_4)_2(Pyz)]\cdot 2CH_3CN$ (X = Cl for **3**, X = Br for **4**) reveal a weak ferromagnetic coupling across the pyrazine bridge between a pair of Mo^V $S = 1/2$ spins. The magnetic properties of $\{(C_2H_5)_4N\}_2[(MoOCl_4)_2(Pyz)]$ (**2**), another compound with dinuclear complex anions, are dominated by antiferromagnetic intermolecular interactions.

Introduction

The $\{MoO\}^{3+}$ entity pervades the chemistry of molybdenum in oxidation state V. Mononuclear Mo^V complexes are relatively rare: two $\{MoO\}^{3+}$ entities are usually linked with one or two oxides to form $\{Mo_2O_3\}^{4+}$ or $\{Mo_2O_4\}^{2+}$ cores, respectively.[1] Both types of bridged compounds are diamagnetic. The diamagnetism of the ones containing the $\{Mo_2O_3\}^{4+}$ core has been rationalized in terms of spin pairing through the bridging oxide, whereas the $\{Mo_2O_4\}^{2+}$ compounds owe their diamagnetism to a direct Mo–Mo interaction.[2] For both, there are two variants of the basic structure, differing in the mutual orientation of a pair of terminal oxides (Scheme 1). A strong preference for a *cis* disposition of Mo=O bonds may be observed among the doubly bridged species. The $\{Mo_2O_4\}^{2+}$ species with *cis* arrangement of the terminal oxides (*syn* isomers) have a strongly puckered $Mo(\mu_2\text{-}O)_2Mo$ ring, whereas the *trans* analogues (*anti* isomers) possess a planar ring.[3] Theoretical calculations have shown that the *syn* isomer is stabilized by a direct π-bonding interaction between two Mo=O entities.[4] The calculations have also confirmed the direct Mo–Mo bonding to be more stable in *syn* isomers.[5] The dimensions of the $\{Mo_2O_4\}^{2+}$ unit are normally not affected by the changes in the ligand set nor by the coordination number of the metal.[6,7] In a manner similar to dimetal units with multiple metal–metal bonds such as Mo_2^{4+} or Rh_2^{4+},[8] the $\{Mo_2O_4\}^{2+}$ unit can serve in combinations with multifunctional organic linkers as a building block in the construction of supramolecular arrays. The major drawback for its successful application is a great tendency of metal centres of the $\{Mo_2O_4\}^{2+}$ core to attain a six-numbered coordination, when the amounts of the linkers are small, through the sharing of bridging oxido ligands.[7] Depending on the reaction conditions, the self-assembly can even produce clusters with the same number of building blocks, but with different connectivities among them. A notable example is a series of tetranuclear clusters which display three distinctly different structures of the metal oxide core, either a chain-like $\{Mo_4O_4(\mu_2\text{-}O)_4(\mu_2\text{-}OR)_2\}^{2+}$ (R = alkyl),[9] (ii) a rhombic $\{Mo_4O_4(\mu_3\text{-}O)_2(\mu_2\text{-}O)_2\}^{4+}$[10] or a cube-like $\{Mo_4O_4(\mu_3\text{-}O)_4\}^{4+}$ core.[11] On the other hand, the use of large amounts of ligands, which would effectively suppress the self-assembly, does not allow sufficient control over the reaction outcome. Nevertheless, reactions with

[a] Department of Chemistry and Chemical Technology, University of Ljubljana,
Aškerčeva 5, 1000 Ljubljana, Slovenia
E-mail: barbara.modec@fkkt.uni-lj.si
[b] CNRS, UPR 8641, Centre de Recherche Paul Pascal (CRPP), Equipe "Matériaux Moléculaires Magnétiques",
115 avenue du Dr. Albert Schweitzer, Pessac 33600, France
[c] Université de Bordeaux, UPR 8641,
Pessac 33600, France

Supporting information for this article is available on the WWW under http://dx.doi.org/10.1002/ejic.200900758.

some multifunctional ligands were met with success. For instance, carboxylate-based ligands linked pairs of $\{Mo_2O_4\}^{2+}$ units into discrete tetranuclear species.[12,13] The carboxylate group typically coordinated to a pair of sites within the $\{Mo_2O_4\}^{2+}$ unit which were *trans* to the multiply bonded oxides. Several inorganic ligands such as carbonate, molybdate(VI), phosphate and sulfite also served as linkers in the formation of clusters with complicated compositions and diverse structures.[14] Invariably, the linkers employed were oxygen donor ligands. There is only one example with a bidentate nitrogen donor ligand serving this role, a mixed-valence octanuclear complex with the $[Mo^{V}_6Mo^{VI}_2O_{18}(Pz)_6(PzH)_6]$ (Pz^- = pyrazolate ion) composition.[15] The aim of our research was to use other multifunctional nitrogen donor ligands. Our ligand of choice was pyrazine, the smallest, and hence most rigid, linear aromatic linker. As will be shown presently, in spite of the wide use of pyrazine in the field of supramolecular chemistry,[16] complexes with molybdenum are surprisingly scarce. With the ligand engaged in a bidentate bridging coordination to two molybdenum atoms of two different dinuclear building blocks, larger arrays with interesting architectures and properties could result. Provided these species undergo redox chemistry without the loss of structural integrity, electronic communication between the metal centres could be assessed. Herein we report the preparations, X-ray structures and characterization of a series of novel molybdenum(V) complexes with pyrazine.

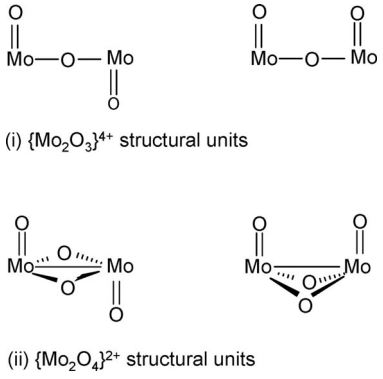

Scheme 1. Dinuclear structural units with *trans* and *cis* arrangements of terminal oxides.

Results and Discussion

Synthetic Considerations

The mononuclear ion $[MoOCl_4(H_2O)]^-$ is labile towards substitution, which makes it an attractive starting material and enables the introduction of various ligands. Under ambient conditions, it reacts with pyrazine to form a series of complexes with pyrazine engaged in monodentate or bidentate bridging coordination. Compounds **1**–**3** which contain a dinuclear anion $[(MoOCl_4)_2(Pyz)]^{2-}$ were obtained from the acetonitrile solutions of $(PyH)_5[MoOCl_4(H_2O)]_3Cl_2$ upon the addition of a stoichiometric amount of pyrazine (Scheme 2). Contrary to expectation, the solutions retained their original emerald green colour after the addition of the nitrogen donor ligand. This indicated that the extent of formation of the oxido-bridged species was negligible.[17] A substitution of the coordinated water molecule for pyrazine and its coordination through both nitrogen atoms generates a dinuclear anion $[(MoOCl_4)_2(Pyz)]^{2-}$. Pyridinium salt of this anion, compound **1**, cocrystallizes with pyridinium chloride.

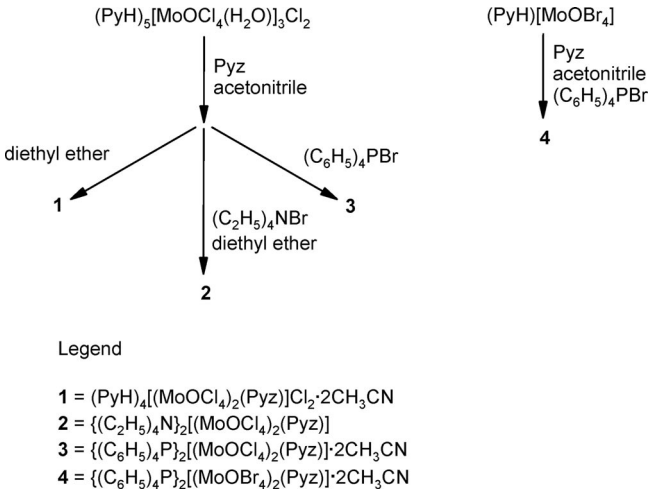

Scheme 2. Syntheses of $[(MoOX_4)_2(Pyz)]^{2-}$ compounds.

Assuming that all the molybdenum is converted into the $[(MoOCl_4)_2(Pyz)]^{2-}$ ion, one third of the latter species remains in solution because of the shortage of both counterions [Equation (1)]. The root of the problem lies in molybdenum starting material being the only source of both metal and counterions, and that their ratio in the product, compound **1**, is changed. In order to improve the yield, pyridinium chloride as an external source of counterions has to be introduced in the reaction mixture.[18] The addition of halide salts of $\{(C_2H_5)_4N\}^+$ or $\{(C_6H_5)_4P\}^+$ ions, as the other option, resulted in the crystallization of $[(MoOCl)_2(Pyz)]^{2-}$ salts with the corresponding cations. For instance, $\{(C_6H_5)_4P\}_2[(MoOCl_4)_2(Pyz)]\cdot 2CH_3CN$ (**3**) was prepared in good yield in a relatively short time. When $(PyH)[MoOBr_4]$ was used as the starting material, a bromide analogue of a dinuclear complex, $\{(C_6H_5)_4P\}_2[(MoOBr_4)_2(Pyz)]\cdot 2CH_3CN$ (**4**), was obtained. With the greater lability of coordinated bromide vs. chloride, a greater extent of substitution within the coordination sphere of the metal was anticipated. A factor that may contribute to the formation of **4** is the ease with which it crystallizes and removes itself from solution. It is to be noted that attempts to prepare mononuclear $[MoOCl_4(Pyz)]^-$ with pyrazine bound in a monodentate manner have not been met with success. Using a large excess of the nitrogen donor ligand, which could theoretically lead to exclusive formation of $[MoOCl_4(Pyz)]^-$, again yielded compound **1** as the only product.

$$2(PyH)_5[MoOCl_4(H_2O)]_3Cl_2 + 3Pyz + 4CH_3CN \rightarrow 2(PyH)_4[(MoOCl_4)_2(Pyz)]Cl_2\cdot 2CH_3CN + [(MoOCl_4)_2(Pyz)]^{2-} + 2PyH^+ + 6H_2O \quad (1)$$

The syntheses of $(PyH)_2[\{MoOCl_3(Pyz)\}_2O]$ (**5**), $(MeNC_5H_5)_2(PyzH_2)[(Mo_2O_4Cl_4)_2(Pyz)_2]$ (**6**) and $(PyH)_4[(Mo_2O_4Cl_4)_2(Pyz)_2]\cdot 2CH_3CN$ (**7**) are not well defined. Either the yields are low or more than one product is formed. Both the dinuclear anion of **5**, $[\{MoOCl_3(Pyz)\}_2O]^{2-}$, and the tetranuclear anions of **6** and **7**, $[(Mo_2O_4Cl_4)_2(Pyz)_2]^{4-}$, contain the bridging oxides. In spite of many known complexes with one or two bridging oxides, the mechanism of their formation remains obscure. Undoubtedly, the key factor is the presence of moisture. A survey of the contents of the reaction mixtures reveals methanol as another common ingredient (Scheme 3). Methanol is known to participate actively in substitution/dimerization reactions through the coordination of the in situ formed methoxide ions. The coordinated methoxide can in turn react with water to form an oxido ligand.[19] On the whole, a substitution of one chloride in molybdenum coordination sphere produces a dinuclear species with a single oxido bridge and three remaining chlorides per metal centre, this being the composition of the anion of $(PyH)_2[\{MoOCl_3(Pyz)\}_2O]$ (**5**). On the other hand, when two halides are replaced, a species with two oxido bridges is formed. Such a reaction probably took place during the formation of $(PyH)_4[(Mo_2O_4Br_4)_2(Pyz)_2]\cdot 2CH_3CN$ (**8**), a $\{Mo_2O_4\}^{2+}$-containing compound, directly from $\{(C_6H_5)_4P\}_2[(MoOBr_4)_2(Pyz)]\cdot 2CH_3CN$ (**4**). An overall reaction is illustrated in Scheme 4. Surprisingly, the molybdenum-to-pyrazine bonds remained intact during the course of the reaction. The isolation of the salt of the $[(Mo_2O_4Br_4)_2(Pyz)_2]^{4-}$ ion speaks in favour of its stability.

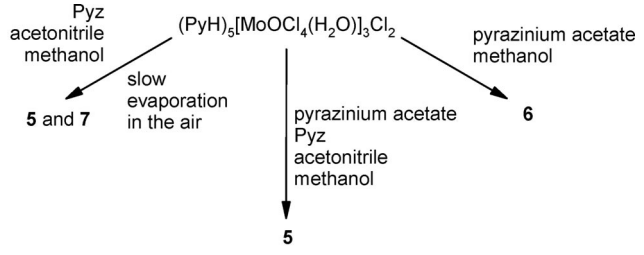

Scheme 3. Syntheses of oxido-bridged compounds **5**–**7**.

The preparation of $(MeNC_5H_5)_2(PyzH_2)[(Mo_2O_4Cl_4)_2(Pyz)_2]$ (**6**) merits further comment. The acetate was introduced with the aim to prepare complexes which would contain both the nitrogen donor ligand and the carboxylate. The preparation of heteroleptic ligand complexes failed. One of the likely reasons is that the acetate was involved in a different reaction. As shown by the composition of the isolated product, it must have reacted with pyridine and methanol to form *N*-methylpyridinium cations. The alkylation of pyridine with alcohol proceeds at elevated temperatures via an intermediate, an ester of carboxylic acid, which subsequently reacts with pyridine.[20] A low yield and a long reaction time encountered in the preparation of **6** have their origin also in the limited extent of the latter reaction under ambient conditions. Efforts to improve the yield or to prepare compound **6** by a more deliberate route were not successful.

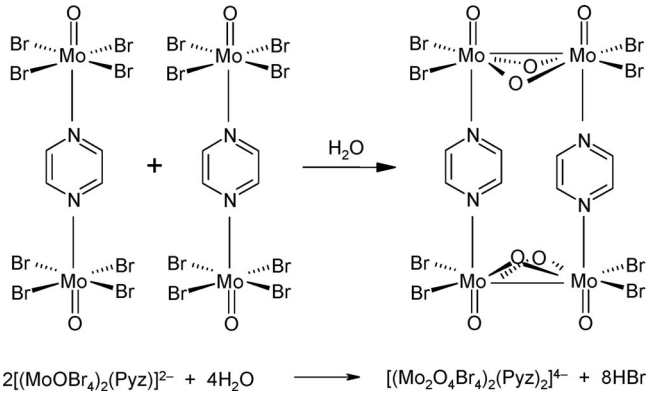

Scheme 4. Formation of $[(Mo_2O_4Br_4)_2(Pyz)_2]^{4-}$, a $\{Mo_2O_4\}^{2+}$-containing species.

Structural Studies

The dinuclear $[(MoOX_4)_2(Pyz)]^{2-}$ (X = Cl, Br) ion, found in $(PyH)_4[(MoOCl_4)_2(Pyz)]Cl_2\cdot 2CH_3CN$ (**1**), $\{(C_2H_5)_4N\}_2[(MoOCl_4)_2(Pyz)]$ (**2**), $\{(C_6H_5)_4P\}_2[(MoOCl_4)_2(Pyz)]\cdot 2CH_3CN$ (**3**) and $\{(C_6H_5)_4P\}_2[(MoOBr_4)_2(Pyz)]\cdot 2CH_3CN$ (**4**), is shown in Figure 1. Relevant geometric parameters are summarized in Table 1. The salts with $\{(C_6H_5)_4P\}^+$ cations, compounds **3** and **4**, are isotypic. The dinuclear anion may be described as two mononuclear $\{MoOX_4\}^-$ entities, linked by the pyrazine ligand, which is engaged in a bidentate bridging coordination. With pyrazine nitrogen atoms occupying positions that are *trans* to the multiply bonded oxides, the molybdenum-to-pyrazine bonds are relatively long: 2.481(2) Å for **1**, 2.474(6) Å for **2**, 2.492(2) Å for **3** and 2.522(2) Å for **4**. Such a distance may suggest that a dinuclear complex is only weakly held together. The lengthening of the bonds *trans* to the terminal oxide is a general phenomenon found throughout the $\{MoO\}^{3+}$ compounds.[1] Also, as a result of the *trans* influence of the Mo=O group, the immediate environment of each molybdenum atom is that of a highly distorted octahedron. Molybdenum is displaced from its octahedral basal plane, that is, the plane of four halido ligands, towards the terminal oxide by ca. 0.36 Å. Consequently, the *cis* angles that incorporate the molybdenyl group are markedly greater than 90°. The mutual orientation of the two $\{MoOX_4\}^-$ subunits within a dianion is such that their halido ligands are exactly superimposed over each other (Figure 1). In order to minimize the steric effects, pyrazine is located roughly in the middle between the halides. Although the centre of gravity of the pyrazine molecule lies on the inversion centre of the $P\bar{1}$ (com-

Table 1. Relevant structural parameters/Å of complexes **1**–**8**.

Compound	Mo–N	Mo–X[a]	Mo–Mo	Mo···Mo[b]
1	2.481(2)	2.3609(5)–2.3866(5)	–	7.7627(3)
2	2.473(6), 2.475(6)	2.367(2)–2.373(2), 2.357(2)–2.380(2)	–	7.7331(9)
3	2.492(3)	2.3664(5)–2.3957(5)	–	7.7877(3)
4	2.522(2)	2.5096(4)–2.5320(3)	–	7.8589(4)
5	2.471(1)	2.3881(5)–2.4258(4)	–	3.7290(3)
6	2.457(3), 2.476(3)	2.4460(12)–2.4616(12)	2.5901(5)	7.6844(5), 8.0932(7)
7	2.472(2), 2.477(2)	2.4482(6)–2.4642(6)	2.6047(3)	7.7136(4), 8.1185(5)
8	2.470(2), 2.471(2)	2.6053(3)–2.6260(3)	2.5976(3)	7.7043(3), 8.1335(4)

[a] X = Cl or Br. [b] Intermetal distances within the anions. Complexes **6**–**8**: a longer side of the Mo_4 rectangle and its diagonal.

pound **1**) or $P2_1/n$ (compounds **3** and **4**) space group, the symmetry of the anion is that of the C_{2h} point group. A twofold rotation axis goes along both Mo=O vectors and bisects the bridging pyrazine in two halves.

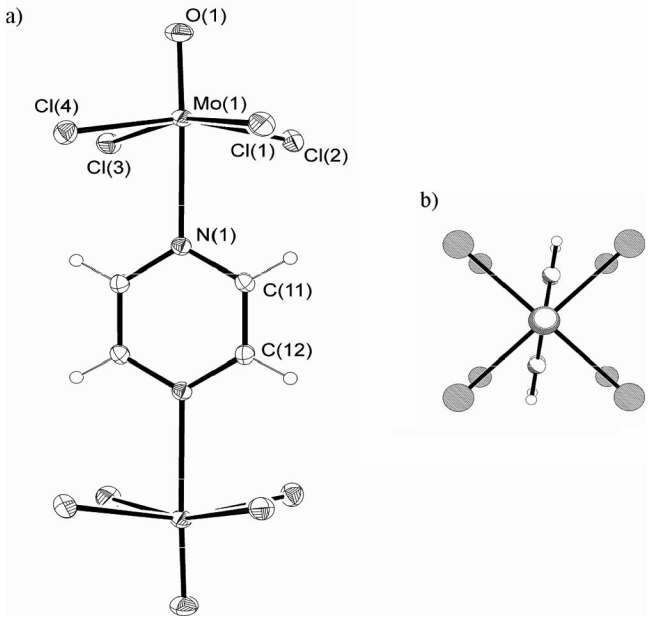

Figure 1. (a) Drawing of $[(MoOCl_4)_2(Pyz)]^{2-}$, the anionic part of **1**. Atoms are represented by displacement ellipsoids at the 30% probability level. Hydrogen atoms are shown as spheres of arbitrary radii. (b) View of the dinuclear anion along the twofold rotation axis.

To the best of our knowledge, a series of $[(MoOX_4)_2(Pyz)]^{2-}$ anions is the second only example of $\{MoOX_4\}^-$ ions linked with a bifunctional ligand into a dinuclear complex. The only other example is $[(MoOCl_4)_2(O,O'\text{-glyme})]^{2-}$, a complex with 1,2-dimethoxyethane.[21] The molybdenum complexes with pyrazine are rather scarce (Table 2).[22] As expected, the listed molybdenum-to-pyrazine bond lengths reflect the relative *trans* influences of the ligands occupying sites opposite to pyrazine.

X-ray structure analysis of $(PyH)_2[\{MoOCl_3(Pyz)\}_2O]$ (**5**) revealed the presence of dinuclear $[\{MoOCl_3(Pyz)\}_2O]^{2-}$ anions (shown in Figure 2) with protonated pyridine molecules as countercations. The anion exhibits a dinuclear structure comprising two identical $\{MoOCl_3(Pyz)\}$ halves linked by a single bridging oxido ligand. With the latter resting upon the inversion centre of the $P2_1/n$ space group, the anion has a C_i symmetry. Consequently, the Mo–O–Mo bridge is linear and symmetrical with Mo–O bond lengths of 1.8645(1) Å. The conformation of the terminal oxides within the $\{Mo_2O_3\}^{4+}$ core is *anti*. The geometric parameters of the $\{Mo_2O_3\}^{4+}$ core are as observed previously.[25] The *cis* angles range from 80.20(3) to 102.66(4)°, and the *trans* angles range from 160.59(1) to 177.02(6)°. The pseudooctahedral environments of the molybdenum atoms, apart from two oxides, consist also of three chlorides with Mo–Cl bond lengths in the range 2.3881(5)–2.4258(4) Å and a monodentate pyrazine ligand with a Mo–N bond length of 2.471(1) Å. Interestingly, the pyrazine ligand in **5** did not realize all its binding abilities in coordination to metal centres. Instead, the other pyrazine nitrogen atom is involved in a hydrogen-bonding interaction with the pyridinium cation (Figure 3).

Table 2. Mo–N bond lengths/Å in related molybdenum complexes with pyrazine.

Complex	Mo–N	Ligand[a]	Ref.
$[\{Mo(NO)(CN)_5\}_2(Pyz)]^{4-}$	2.332(3)	nitrosyl	[16b]
$[MoO(CN)_4(Pyz)]^{2-}$	2.569(3)	oxide	[23]
$[Mo_2O_6(Pyz)]$	2.449(8)	oxide	[24]
$[\{[Rh(cod)]_2[Mo(dtc)]_2(\mu_3\text{-}S)_4\}_2(Pyz)_2]^{4+}$ [b]	2.439(6), 2.448(5)	sulfide	[16g]

[a] The ligand bound to a site which is *trans* to pyrazine. [b] cod = 1,5-cyclooctadiene, dtc = diethyldithiocarbamate.

The tetranuclear $[(Mo_2O_4X_4)_2(Pyz)_2]^{4-}$ (X = Cl, Br) ion, found in $(MeNC_5H_5)_2(PyzH_2)[(Mo_2O_4Cl_4)_2(Pyz)_2]$ (**6**), $(PyH)_4[(Mo_2O_4Cl_4)_2(Pyz)_2]\cdot 2CH_3CN$ (**7**) and $(PyH)_4[(Mo_2O_4Br_4)_2(Pyz)_2]\cdot 2CH_3CN$ (**8**), is shown in Figure 4. The anion is a tetranuclear cluster that may be viewed as two identical dinuclear $\{Mo_2O_4X_4\}^{2-}$ subunits, bridged by a pair of bidentate pyrazines. The molybdenum-to-pyrazine bond lengths are comparable to those observed for complexes **1**–**5**. The two halves are related by the inversion centre located in the centre of the Mo_4 rectangle. The overall symmetry of the tetraanion is much higher: it closely approaches that of the D_{2h} point group. The individual dinuclear subunits contain the *syn*-$\{Mo_2O_4\}^{2+}$ core, whose Mo^V centres participate in a metal–metal bond with intermetal distances of 2.5901(5) Å for **6**, 2.6047(3) Å for **7** and 2.5976(3) Å for **8**. This bond length corresponds to a single metal–metal bond.[7a] As usually observed, the $Mo(\mu_2\text{-}O)_2Mo$ ring of the $\{Mo_2O_4\}^{2+}$ core is not planar. Its deviation from planarity may be expressed with a dihedral

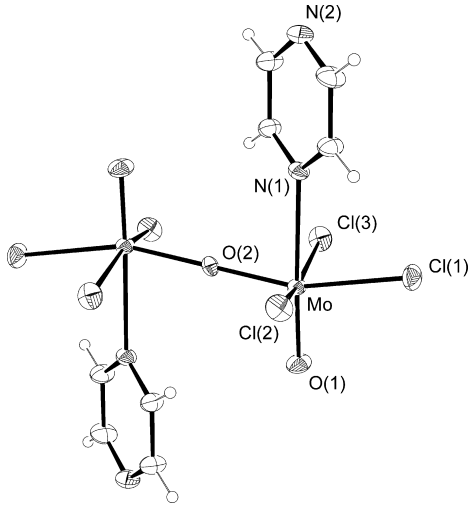

Figure 2. Drawing of $[\{MoOCl_3(Pyz)\}_2O]^{2-}$, the anionic part of **5**. Atoms are represented by displacement ellipsoids at the 30% probability level.

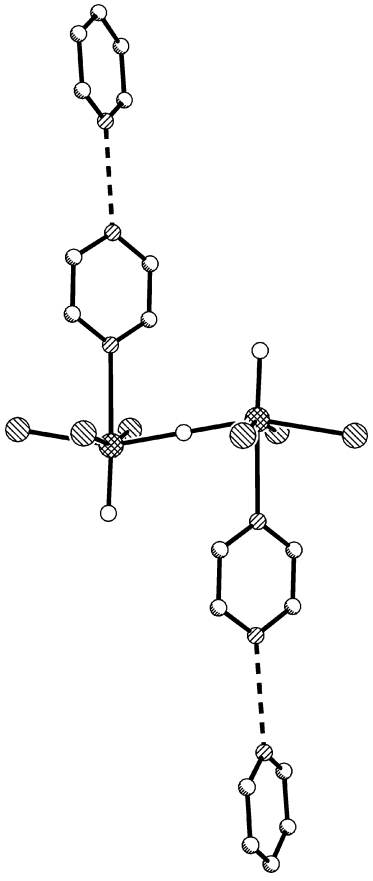

Figure 3. A dinuclear anion of **5** with a pair of hydrogen-bonded pyridinium cations. The corresponding N···N distances are 2.822(2) Å.[26] Hydrogen atoms are omitted for clarity.

angle between two $Mo(\mu_2\text{-}O)_2$ planes, denoted shortly as a fold angle. Despite the rather weak binding of pyrazine, the $\{Mo_2O_4\}^{2+}$ cores of the anions of **6**–**8** display subtle changes in their internal geometry (Table 3). Apparently, a more pronounced puckering of the $Mo_2(\mu_2\text{-}O)_2$ bridge in **6**–**8**, as compared to that in discrete dinuclear $\{Mo_2O_4\}^{2+}$ species, is counterweighted by the contraction of the O–Mo–O angles. Similar changes were observed for the constituent dinuclear units of $[Mo_4O_8(C_4O_4)_4]^{4-}$ with a cube-like metal-oxide framework.[11d] On the other hand, the $\{Mo_2O_4\}^{2+}$ units of three other tetranuclear complexes, $[\{Mo_2O_4(\eta^2\text{-}C_2O_4)_2\}_2(\mu_4\text{-}C_2O_4)]^{6-}$,[13] $[(Mo_2O_4Cl_4)_2(\mu_4\text{-}hda)]^{6-}$ and $[\{Mo_2O_4(Py)_3\}_2(\mu_3\text{-}btcH)_2]$,[12] display changes of the opposite sign: a more planar bridge with somewhat widened O–Mo–O angles. It remains to be noted that the resulting Mo–Mo bond lengths, also listed in Table 3, are influenced mainly by the electron withdrawing/donating nature of the ligands surrounding the pair of metal atoms. The rather long Mo–Mo bonds in **6**–**8** thus find their origin in the high content of halido ligands whose nature is electron withdrawing.

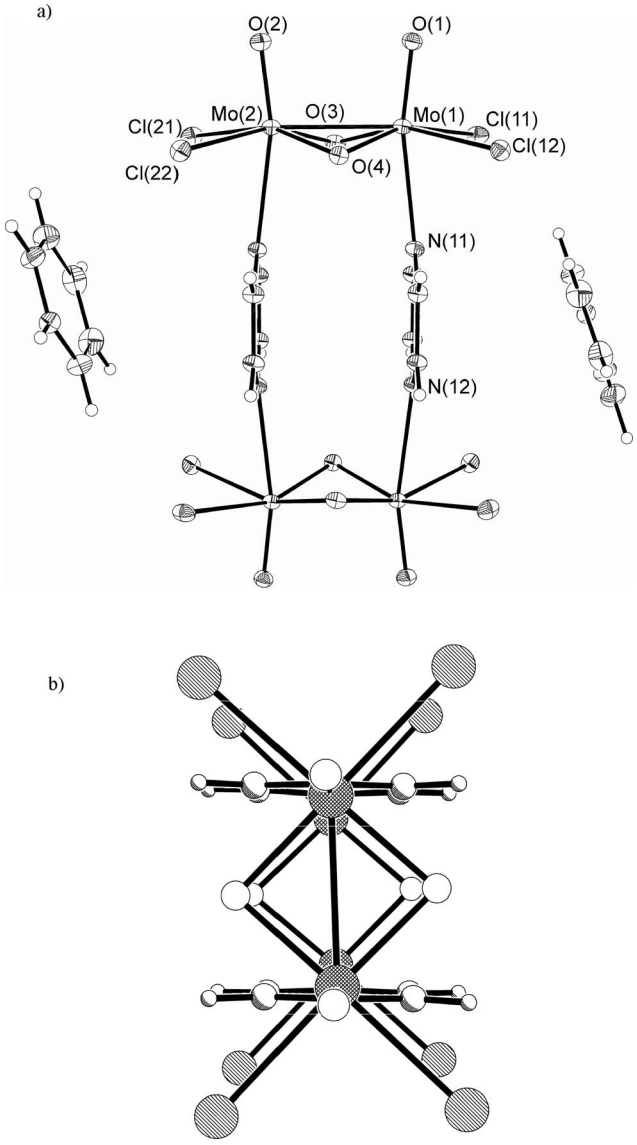

Figure 4. (a) Drawing of $[(Mo_2O_4Cl_4)_2(Pyz)_2]^{4-}$, the anionic part of **7**, with a pair of PyH^+ ions. Atoms are represented by displacement ellipsoids at the 30% probability level. (b) View of the tetranuclear anion along the Mo=O vectors.

Table 3. Internal dimensions of $\{Mo_2O_4\}^{2+}$ cores in selected dinuclear and tetranuclear complexes.

	Mo–Mo / Å	Fold angle / °	Mo–O–Mo / °	O–Mo–O / °	Ref.
6	2.5901(5)	142.3(1)	82.74(1), 83.9(1)	90.6(1), 90.9(1)	this work
7	2.6047(3)	142.8(1)	83.51(6), 83.68(6)	90.58(7), 90.68(7)	this work
8	2.5976(3)	142.98(7)	83.40(7)	90.85(7), 90.95(8)	this work
$[Mo_2O_4(glyc)_2(Py)_2]^{2-}$ [a,b]	2.5593(4)	154.81(5)	82.69(7)	94.80(7)	[27]
$[Mo_2O_4(\eta^2\text{-}C_2O_4)_2(Py)_2]^{2-}$ [a]	2.5468(4)	149.62(6)	82.16(9), 82.29(9)	94.0(1), 94.2(1)	[13]
$[Mo_4O_8(C_4O_4)_4]^{4-}$ [c]	2.5904(4)	138.02(6)	81.78(8), 81.85(8)	89.12(9), 89.35(8)	[11d]
	2.5932(4)	133.84(6)	82.02(7)	89.8(1), 90.2(1)	
$[\{Mo_2O_4(\eta^2\text{-}C_2O_4)_2\}_2(\mu_4\text{-}C_2O_4)]^{6-}$ [d]	2.5655(4)	160.21(5)	82.73(7)	95.73(7)	[13]
$[(Mo_2O_4Cl_4)_2(\mu_4\text{-hda})]^{6-}$ [d,e]	2.5824(3)	159.9(1)	82.84(6), 82.95(7)	95.21(7), 95.82(7)	[12]
$[\{Mo_2O_4(Py)_3\}_2(\mu_3\text{-btcH})_2]$ [f]	2.5326(3)	160.1(1)	81.53(8), 81.97(8)	96.50(9), 96.95(9)	[12]
	2.5410(3)	160.4(1)	81.87(8), 82.21(8)	96.42(9), 96.54(9)	

[a] Dinuclear species. [b] $glyc^{2-}$ = glycolate ion, $^{-}OCH_2COO^{-}$. [c] Contains a cube-like $\{Mo_4O_4(\mu_3\text{-}O)_4\}^{4+}$ core obtained upon the self-assembly of two $\{Mo_2O_4\}^{2+}$ units. [d] A dicarboxylate ion bridges two $\{Mo_2O_4\}^{2+}$ units. Each carboxylate group is coordinated to a pair of *trans* positions of the $\{Mo_2O_4\}^{2+}$ unit. [e] hda^{2-} = heptanedioate. [f] Two $btcH^{2-}$ ions (1,3,5-benzenetricarboxylic acid with two deprotonated carboxylic groups) link two $\{Mo_2O_4\}^{2+}$ units. See ref.[12] for their binding mode.

The rectangular Mo_4 array of the $[(Mo_2O_4X_4)_2(Pyz)_2]^{4-}$ anion has two short, ca. 2.6 Å, and two long Mo–Mo distances, ca. 7.7 Å (Table 1). As shown in Figure 4, the longer sides of the Mo_4 rectangle are bowed outward with the planes of the bridging pyrazines being exactly parallel to each other and the separation between them being on the average 3.2 Å.[28] Such a short distance is indicative of a strong π–π stacking interaction. The stacked, face-to-face arrangements with perfect alignment of aromatic planes are not very common.[29] The pyrazine ligands of all three compounds participate in another π–π type interaction. For instance in **7**, the interaction occurs with a pyridinium cation whose plane is tilted away from pyrazine by ca. 20°. The centroid–centroid distance of 3.9 Å implies a significantly weaker interaction than the one occurring between a pair of coordinated pyrazines, but still not a negligible one. As a result, the tetranuclear anion is sandwiched between a pair of aromatic cations. In a similar manner, the pyrazine bridges of **6** interact with *N*-methylpyridinium cations (Figure S3, Supporting Information). The π–π-type interactions probably contribute to the overall stability of the tetranuclear array.

Magnetic Properties of the $[(MoOX_4)_2(Pyz)]^{2-}$ Compounds

The magnetic susceptibility measurements as a function of temperature for compounds **2**, **3** and **4** are shown as χT vs. T plots (Figure 5). The room-temperature χT product, 0.64 $cm^3\,K\,mol^{-1}$ for **2** and **3** and 0.73 $cm^3\,K\,mol^{-1}$ for **4**, is in good agreement with the presence of two $S = 1/2$ spins. Upon lowering the temperature, the value of χT is roughly constant down to 70 K for all three compounds. With further lowering to 1.8 K, the value of the χT product increases for **3** and **4**, whereas it decreases for **2**. At 1.8 K, the value of the χT product amounts to 0.59, 0.72 and 0.85 $cm^3\,K\,mol^{-1}$ for **2**, **3** and **4**, respectively. Such thermal behaviour is typically observed for paramagnetic complexes which possess weak magnetic interactions between the spin carriers. On the basis of the crystal structure, a simple Heisenberg $S = 1/2$ dinuclear model was used to fit the magnetic susceptibility considering the following spin Hamiltonian: $H = -2J\{\boldsymbol{S}_{Mo1}\cdot\boldsymbol{S}_{Mo2}\}$ (where $\boldsymbol{S}_{Mo1}$ and $\boldsymbol{S}_{Mo2}$ are the spin operators with $S_{Mo1} = S_{Mo2} = 1/2$).[30] As shown in Figure 5, the experimental data are very well reproduced by this theoretical approach with the best sets of parameters being: $J/k_B = -0.39(5)$ K and $g = 1.86(2)$ for **2**; $J/k_B = +0.49(5)$ K and $g = 1.86(2)$ for **3** and $J/k_B = +0.57(5)$ K and $g = 1.99(2)$ for **4**. The average g factor for the $[(MoOCl_4)_2(Pyz)]^{2-}$ unit is found reproducibly around 1.86, while the bromide analogue displays a much closer value to 2. The most important difference among the three compounds is certainly related to the magnetic interactions. While ferromagnetic interactions are observed for **3** and **4**, the dominant interactions present in **2** are antiferromagnetic. It should be noted that these magnetic behaviours were reproducibly observed for different batches of the samples. It seems unlikely, for the reasons that follow, that the antiferromagnetic interactions observed for **2** are intramolecular by nature. The packing arrangements for **3** and **4** are such that the $[(MoOX_4)_2(Pyz)]^{2-}$ ions are extremely well separated from each other by the bulky $\{(C_6H_5)_4P\}^{+}$ cations, thereby suggesting the absence of any significant interactions between the dinuclear ions. This strongly supports the nature of the intramolecular interaction between Mo^{V} $S = 1/2$ spins in this type of complex to be ferromagnetic. As the geometric parameters of the $[(MoOX_4)_2(Pyz)]^{2-}$ ions in the three compounds are extremely similar, there is no reason for a change in the nature of the intramolecular interaction in the case of compound **2** which should also possess intramolecular ferromagnetic interactions. The antiferromagnetic behaviour observed for **2** is probably a result of intermolecular interactions that are stronger and thus overcome the intracomplex ferromagnetic ones. This hypothesis is supported by the packing of the $[(MoOCl_4)_2(Pyz)]^{2-}$ ions in **2**. The presence of small $\{(C_2H_5)_4N\}^{+}$ cations allows closer approach of the dinuclear ions with $Cl_4Mo{=}O\cdots O{=}MoCl_4$ contacts of about 4.4 Å, which could mediate these antiferromagnetic interactions. Unfortunately due to the small amplitude of both the intra- and intermo-

lecular interactions, it has not been possible to verify this hypothesis by more detailed analysis of the magnetic properties, which would allow separate determination of both types of interactions.

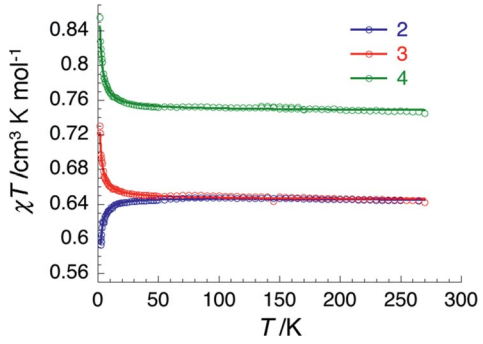

Figure 5. χT vs. T plots (with χ being the magnetic susceptibility equal to M/H) for **2** (blue), **3** (red) and **4** (green), measured at 1000 Oe. The solid lines are the best-fit lines obtained with the Heisenberg $S = 1/2$ dimer model described in the text.

Electrochemical Properties of the $[(MoOX_4)_2(Pyz)]^{2-}$ Compounds

The electrochemical experiments were undertaken with the aim to evaluate the electronic communication between a pair of metal centres in the $[(MoOX_4)_2(Pyz)]^{2-}$ ions. Cyclic voltammetry of $\{(C_2H_5)_4N\}_2[(MoOCl_4)_2(Pyz)]$ (**2**) in DMF revealed an irreversible reduction at –1.022 V with oxidation at –0.218 V vs. Ag/AgCl (Figure 6). The electrochemical behaviour of $\{(C_6H_5)_4P\}_2[(MoOCl_4)_2(Pyz)]\cdot 2CH_3CN$ (**3**) was practically the same as that of **2**. The peak currents of the reduction and oxidation waves depended linearly on the square root of the scan rate, thus indicating a diffusion-controlled reaction. By starting at –0.500 V and scanning in the positive direction, no oxidation was observed. If a small amount of pyrazine was added to the solution of **2**, the CV trace remained unchanged. The reduction at –1.022 V has to be metal centred and was assigned as a Mo^{V}/Mo^{IV} couple. In view of the rather weak binding of pyrazine in $[(MoOCl_4)_2(Pyz)]^{2-}$, the cleavage of molybdenum-to-pyrazine bonds with the ensuing formation of mononuclear fragments seems highly feasible. The presence of mononuclear Mo^{V} species provides an adequate explanation for a single reduction wave. Furthermore, the electrochemical behaviour of a mononuclear Mo^{V} complex, $\{(C_2H_5)_4N\}[MoOCl_4(H_2O)]$, was exactly the same as that of **2**.[31] For a dinuclear complex with bromide, $\{(C_6H_5)_4P\}_2[(MoOBr_4)_2(Pyz)]\cdot 2CH_3CN$ (**4**), reduction waves at –0.390 and –1.000 V with oxidations at –0.7168 and –0.2055 V were observed (Figure 7). By analogy, the CV trace of a mononuclear complex, $\{(C_2H_5)_4N\}[MoOBr_4(H_2O)]$, was identical and as such confirmed the rupture of a dinuclear structure in the solution. Position of the Mo^{V} reduction is almost the same as for the chloride analogue, whereas the corresponding oxidation is at a more negative potential, at –0.7168 V. This indicates that the reduced species with coordinated bromide is easier to oxidize than its chloride counterpart. A reduction wave at –0.390 V is probably related to H^{+} ions.[32] This raises a question of their source. It is well known that the substitution of halides in the molybdenum coordination sphere results in the lowering of the pH. Apparently, this process is of a greater importance for Mo^{V} complexes with a more labile bromide than for the chloride analogues.

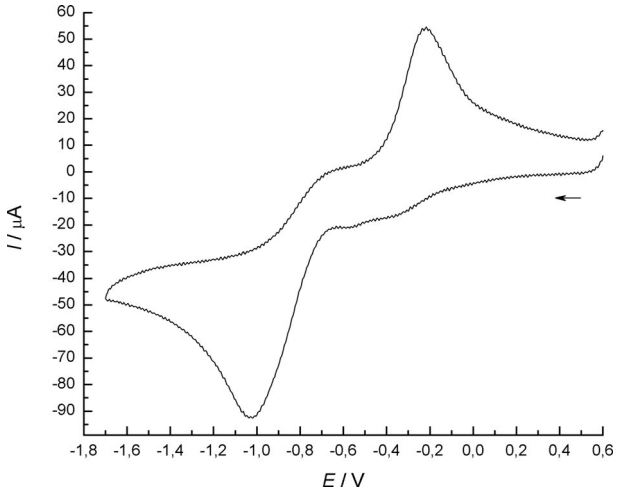

Figure 6. Cyclic voltammogram of **2** in DMF at a scan rate of 100 mV s^{-1}.

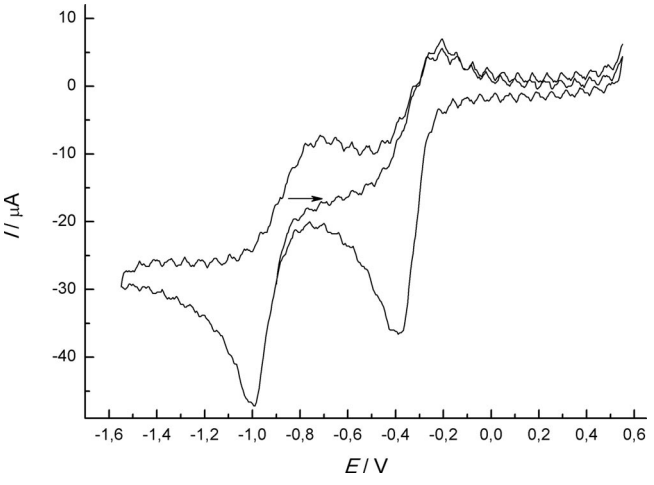

Figure 7. Cyclic voltammogram of **4** in DMF at a scan rate of 50 mV s^{-1}.

Electronic Spectra

The visible spectra of the solutions of compounds containing the $[(MoOCl_4)_2(Pyz)]^{2-}$ ions are very similar to those of $\{(C_2H_5)_4N\}[MoOCl_4(H_2O)]$, which possesses mononuclear complex ions.[33] This adds further proof that the dinuclear structure does not retain its integrity in solution.[34]

The spectrum of the crystalline $(PyH)_2[\{MoOCl_3(Pyz)\}_2O]$ (**5**) suspended in Nujol is characterized by an absorption at 478 nm with a shoulder at 512 nm. This band is assigned to the electronic transition involving a linear Mo–O–Mo bridging unit.[1a] Depending on the ligand set, the $\{Mo_2O_3\}^{4+}$ complexes exhibit bands in the 450–525 nm range.[35] The solution of $(PyH)_2[\{MoOCl_3(Pyz)\}_2O]$ (**5**) in DMF displayed rapid colour changes: the initially purple brown solution turned yellow within half an hour.[36] Decomposition of **5** is likely to proceed via disproportionation to $\{Mo^{IV}O\}^{2+}$ and $\{Mo^{VI}O_2\}^{2+}$ species. The latter process is known to be highly favoured for compounds with the $\{Mo_2O_3\}^{4+}$ core.[37]

Infrared Spectroscopy

Infrared spectra of compounds **1**–**8** display a complex pattern of features between 1650 and 400 cm^{-1} that are associated with the presence of coordinated pyrazine and countercations. The complexity of the spectra precludes the exact assignments of either. With the absorptions of the Mo=O bonds often being the strongest in the spectrum, they can serve as a potent diagnostic for the presence of $\{MoO\}^{3+}$ moieties.[1a,38] Accordingly, the spectra of the title compounds exhibit intense bands in the 980–960 cm^{-1} range. Strong absorptions at 758 and 433 cm^{-1} in the spectrum of **5**, a species with the $\{Mo_2O_3\}^{4+}$ core, may be attributed to the ν_{as}(Mo–O–Mo) and δ(Mo–O–Mo) vibrations.[39] Absorptions associated with the Mo–O–Mo vibrations of the $\{Mo_2O_4\}^{2+}$ cores appear as intense bands at 717 and 475 cm^{-1} for **6**, at 753, 716 and 473 cm^{-1} for **7** and at 750, 704 and 473 cm^{-1} for **8**. Weak absorption band at ca. 2250 cm^{-1} in the spectra of **1**, **3**, **4**, **7** and **8** confirms the presence of acetonitrile solvent molecules. Its intensity diminishes with time. The band has its origin in the triple bond stretching vibration which occurs in aliphatic nitriles in the 2260–2240 cm^{-1} range.[40]

Conclusions

The main finding of our work is the preparation, under mild conditions, and the full characterization of a series of molybdenum(V) complexes with pyrazine. The series includes several of the frequently occurring structural cores in molybdenum(V) coordination chemistry: $\{MoO\}^{3+}$, *anti*-$\{Mo_2O_3\}^{4+}$ and *syn*-$\{Mo_2O_4\}^{2+}$. In all complexes, pyrazine is coordinated to a position *trans* with respect to the molybdenyl group. In $[\{MoOCl_3(Pyz)\}_2O]^{2-}$, a dinuclear complex with a bridging oxide, pyrazine has engaged in coordination only one nitrogen donor atom. In all other complexes, pyrazine has realized all its binding abilities in coordination to the metal centres. Dimerization of the $\{MoOX_4\}^-$ (X = Cl, Br) anions or the $\{Mo_2O_4X_4\}^{2-}$ dianions via one or two bidentate pyrazine ligands generated novel anionic complexes $[(MoOX_4)_2(Pyz)]^{2-}$ and $[(Mo_2O_4X_4)_2(Pyz)_2]^{4-}$. Dinuclear $[(MoOX_4)_2(Pyz)]^{2-}$ ions are rare examples of a linkage of mononuclear entities with bifunctional ligands. The $[(MoOX_4)_2(Pyz)]^{2-}$ ions display intramolecular ferromagnetic interactions leading to an $S = 1$ spin ground state. The highly symmetrical, tetranuclear $[(Mo_2O_4X_4)_2(Pyz)_2]^{4-}$ anions are the second only example of a linkage of metal–metal bonded $\{Mo_2O_4\}^{2+}$ building blocks with nitrogen donor ligands as the connectors. Efforts to expand this chemistry to other multifunctional nitrogen donor ligands are in progress.

Experimental Section

General: All manipulations were conducted in air. Chemicals were purchased from Aldrich and used as received. $(PyH)_5[MoOCl_4(H_2O)]_3Cl_2$ and $(PyH)[MoOBr_4]$ were prepared following published procedures.[17] Pyridinium chloride or bromide was prepared by neutralizing a corresponding acid with pyridine, followed by vacuum drying. Elemental analyses were performed by the Chemistry Department service at the University of Ljubljana. Infrared spectra were measured on Nujol mulls or directly on solid samples by using a Golden Gate ATR with a Perkin–Elmer Spectrum 100 spectrometer. Electronic spectra were obtained with a Cary 50 Probe spectrophotometer at concentrations from 1.25×10^{-4} to 2.5×10^{-3} M by using 1-cm matched quartz cells. The molar absorptivities were calculated by using a total metal concentration. The spectrum of solid **5** suspended in Nujol mull was acquired with a Perkin–Elmer UV/Vis/NIR Lambda 19 spectrophotometer following the technique described by Cotton et al.[41] ^1H NMR spectra of [D$_6$]DMSO solutions were recorded with a Bruker Avance DPX 300 spectrometer, with chemical shifts (δ) referenced to tetramethylsilane. Magnetic susceptibility data were obtained with the use of a Quantum Design SQUID magnetometer MPMS-XL, which works between 1.8 and 400 K for dc applied fields ranging from –7 to 7 T. Measurements were performed on polycrystalline samples with masses of 51.42, 37.50 and 22.5 mg for **2**, **3** and **4**, respectively. The absence of ferromagnetic impurities was checked by measuring the magnetization as a function of the dc field at 100 K. The magnetic data were corrected for the sample holder and the diamagnetic contribution. The cyclic voltammograms of the complexes (1.0 mM in DMF) were recorded with an EG & G instrument, Princeton Applied Research Potentiostat/Galvanostat Model 283, with nBu$_4$NBr (0.1 M) electrolyte, Pt working (platinum disc, 0.126 cm^2) and auxiliary (Pt wire) electrodes and a Ag/AgCl reference electrode. The solutions were deaerated prior to each measurement, and an argon atmosphere was maintained inside the cell throughout the measurement. All the potential values are referred to the Ag/AgCl electrode. Under the experimental conditions used, the $E_{1/2}$ of the ferrocenium/ferrocene couple occurred consistently at –0.675 V. TGA analyses of compounds **3** and **4** were performed with a thermogravimetric analyzer Mettler TGA-SDTA 851^e under 20 mL min^{-1} of flowing argon with a heating rate of 5 °C min^{-1} from 25 to 800 °C. The decomposition products were investigated by X-ray powder diffraction. XRPD data were collected with a PANalytical X'Pert PRO MPD diffractometer by using Cu-K_{α_1} radiation (λ = 1.5406 Å).

$(PyH)_4[(MoOCl_4)_2(Pyz)]Cl_2 \cdot 2CH_3CN$ (1): Pyrazine (50 mg, 0.62 mmol) was added to a solution of $(PyH)_5[MoOCl_4(H_2O)]_3Cl_2$ (428 mg, 1.0 mmol of Mo) in acetonitrile (20 mL). An emerald green solution was obtained. Diethyl ether (5 mL) was added to this solution. The obtained solution was left to stand in a closed Erlenmeyer flask under ambient conditions. A copious amount of green crystals of **1** was obtained after 2 d. Yield: 136 mg (26%). The crystals of **1** became opaque when removed from the mother

liquor. Dried sample: $C_{24}H_{28}Cl_{10}Mo_2N_6O_2$ (978.9): calcd. C 29.45, H 2.88, N 8.58; found C 29.56, H 2.97, N 8.43. IR: $\tilde{\nu}$ = 2252 (w), 1635 (m), 1608 (s), 1532 (s), 1484 (s), 1413 (m), 1408 (s), 1375 (s), 1306 (w), 1248 (w), 1197 (w), 1163 (m), 1149 (m), 1126 (w), 1117 (m), 1078 (w), 1052 (vs), 1005 (w), 978 (vvs, $\nu_{Mo=O}$), 941 (m), 893 (m), 804 (m), 744 (vvvs), 722 (vvs), 676 (vvs), 608 (m), 476 (vs) cm^{-1}.

$\{(C_2H_5)_4N\}_2[(MoOCl_4)_2(Pyz)]$ (2): Pyrazine (50 mg, 0.62 mmol) was added to a solution of $(PyH)_5[MoOCl_4(H_2O)]_3Cl_2$ (428 mg, 1.0 mmol of Mo) in acetonitrile (20 mL). After 30 min, tetraethylammonium bromide (240 mg, 1.14 mmol) was added to this solution. A small container filled with diethyl ether (5 mL) was carefully inserted into the flask with the reaction mixture. The flask was stoppered and stored in the refrigerator at 5 °C. Green crystals of **2** were obtained after 2 d. Yield: 162 mg (38%). $C_{20}H_{44}Cl_8Mo_2N_4O_2$ (848.1): calcd. C 28.32, H 5.23, N 6.61; found C 28.36, H 5.32, N 6.56. IR: $\tilde{\nu}$ = 3109 (w), 3096 (w), 2990 (w), 1485 (m), 1459 (s), 1415 (vs), 1399 (s), 1304 (m), 1183 (s), 1154 (s), 1122 (s), 1077 (w), 1053 (vs), 1031 (m), 1003 (m), 977 (vvs, $\nu_{Mo=O}$), 940 (m), 895 (m), 816 (s), 790 (s), 722 (w), 481 (s) cm^{-1}. UV/Vis (DMF): λ (ε / $L\,mol^{-1}\,cm^{-1}$) = 455 (25), 745 (20) nm.

$\{(C_6H_5)_4P\}_2[(MoOCl_4)_2(Pyz)]\cdot 2CH_3CN$ (3): Pyrazine (50 mg, 0.62 mmol) was added to a solution of $(PyH)_5[MoOCl_4(H_2O)]_3Cl_2$ (428 mg, 1.0 mmol of Mo) in acetonitrile (20 mL). After 30 min, tetraphenylphosphonium bromide (461 mg, 1.10 mmol) was added to this solution. An emerald green solution was left to stand in a closed Erlenmeyer flask under ambient conditions. Within 1 h, light green crystals of **3** started to deposit. The product was filtered off on the following day. Yield: 492 mg (73%). $C_{56}H_{50}Cl_8Mo_2N_4O_2P_2$ (1348.4): calcd. C 49.88, H 3.74, N 4.15; found C 49.61, H 3.71, N 4.32. IR: $\tilde{\nu}$ = 1586 (m), 1416 (s), 1316 (m), 1188 (m), 1164 (w), 1154 (w), 1129 (m), 1107 (vvs), 1050 (vs), 1027 (w), 995 (s), 979 (vvs, $\nu_{Mo=O}$), 938 (m), 921 (w), 895 (m), 849 (w), 798 (s), 763 (vs), 756 (vs), 722 (vvs), 692 (vvs), 615 (m), 525 (vvs), 476 (vs), 454 (m), 434 (w) cm^{-1}. UV/Vis (DMF): λ (ε / $L\,mol^{-1}\,cm^{-1}$) = 365 (sh., 340), 455 (20), 745 (15) nm. TG: A sharp weight loss of 6.6% in the 80–100 °C temperature interval corresponds to the release of the acetonitrile molecules of crystallization (theoretical: 6.1%). The loss of pyrazine takes place between 130 and 190 °C (6.1% weight loss, 5.9% predicted) and is followed by a three-step degradation which commences at ca. 210 °C. The final mass remnant at 800 °C (22.4% of the original) roughly correlates with that calculated for MoO_2 (19.0%). The final decomposition product is MoO_2, as shown by X-ray powder diffraction.

$\{(C_6H_5)_4P\}_2[(MoOBr_4)_2(Pyz)]\cdot 2CH_3CN$ (4): Pyrazine (90 mg, 1.12 mmol) was added to a solution of $(PyH)[MoOBr_4]$ (511 mg, 1.0 mmol of Mo) in acetonitrile (20 mL). Tetraphenylphosphonium bromide (505 mg, 1.20 mmol) was added to this solution. A solution of gold colour was left to stand in a closed Erlenmeyer flask under ambient conditions. Large, brown-yellow crystals of **4** were filtered off on the following day. Yield: 235 mg (28%). $C_{56}H_{50}Br_8Mo_2N_4O_2P_2$ (1704.1): calcd. C 39.47, H 2.96, N 3.29; found C 39.25, H 2.79, N 3.11. IR: $\tilde{\nu}$ = 2252 (m), 1586 (s), 1484 (s), 1434 (vvs), 1415 (s), 1370 (w), 1317 (w), 1188 (m), 1163 (w), 1129 (m), 1107 (vvs), 1048 (s), 1027 (w), 996 (s), 976 (vvs, $\nu_{Mo=O}$), 797 (s), 762 (s), 755 (s), 722 (vvs), 689 (vvs), 615 (w), 533 (w), 525 (vvs), 476 (m), 454 (w) cm^{-1}. UV/Vis (DMF): λ (ε / $L\,mol^{-1}\,cm^{-1}$) = 315 (2100), 755 (90) nm. TG: A sharp weight loss of 5.0% in the 90–110 °C temperature interval corresponds to the release of the acetonitrile molecules of crystallization (theoretical: 4.8%). The loss of pyrazine takes place between 125 and 170 °C (4.7% weight loss, 4.7% predicted). There is a plateau of stability from 170 to 290 °C, followed by a sharp decrease of weight. The final mass remnant at 800 °C is 19.6% (theoretical for MoO_2: 15.0%). The final decomposition product is MoO_2, as shown by X-ray powder diffraction.

$(PyH)_2[\{MoOCl_3(Pyz)\}_2O]$ (5): A freshly prepared solution of pyrazinium acetate (1.20 M in acetonitrile, 5.0 mL, 6.0 mmol) was added to acetonitrile (10 mL) and methanol (3 mL). To this solution was added pyrazine (160 mg, 2.0 mmol), followed by the addition of $(PyH)_5[MoOCl_4(H_2O)]_3Cl_2$ (600 mg, 1.4 mmol of Mo). A solution of red colour was left to stand in a closed Erlenmeyer flask under ambient conditions. Brown crystals of **5** were filtered off after 4 d. Yield: 66 mg (12%). $C_{18}H_{20}Cl_6Mo_2N_6O_3$ (773.0): calcd. C 27.92, H 2.60, N 10.86; found C 28.06, H 2.62, N 10.73. IR: $\tilde{\nu}$ = 1634 (s), 1603 (w), 1550 (m), 1490 (vvs), 1420 (vvs), 1397 (m), 1346 (m), 1252 (m), 1228 (m), 1208 (w), 1166 (s), 1156 (vs), 1130 (vs), 1081 (m), 1046 (vs), 1024 (m), 1002 (m), 959 (vvs, $\nu_{Mo=O}$), 802 (vvs), 790 (vvs), 758 (vvs), 748 (vvs), 722 (vs), 679 (vvs), 639 (m), 602 (vs), 456 (vvs), 433 (vvs) cm^{-1}. UV/Vis (DMF): λ = 312, 458, 761 nm. No molar absorptivities are given due to rapid colour changes of the solution. UV/Vis (Nujol): λ = 464, 505 nm. ^1H NMR (300 MHz, [D$_6$]DMSO): δ = 8.04 [m, 4 H, $H^{3,5}$(PyH$^+$)], 8.57 [t, J = 7.9 Hz, 2 H, H^4(PyH$^+$)], 8.67 (s, 8 H, Pyz), 8.92 [d, J = 6.0 Hz, 4 H, $H^{2,6}$(PyH$^+$)] ppm.

$(MeNC_5H_5)_2(PyzH_2)[(Mo_2O_4Cl_4)_2(Pyz)_2]$ (6): A freshly prepared solution of pyrazinium acetate (1.20 M in acetonitrile, 1.0 mL, 1.2 mmol) was added to methanol (4 mL), followed by the addition of $(PyH)_5[MoOCl_4(H_2O)]_3Cl_2$ (400 mg, 0.93 mmol of Mo). A solution of red colour was left to stand in a closed Erlenmeyer flask under ambient conditions. Orange crystals of **6** deposited from the solution within 2 weeks. Yield: 43 mg (15%). $C_{24}H_{30}Cl_8Mo_4N_8O_8$ (1225.9): calcd. C 23.42, H 2.46, N 9.11; found C 23.66, H 2.61, N 9.08. IR: $\tilde{\nu}$ = 1632 (w), 1604 (m), 1534 (m), 1413 (s), 1211 (w), 1181 (m), 1164 (s), 1124 (s), 1053 (vs), 1017 (w), 960 (vvs, $\nu_{Mo=O}$), 903 (w), 827 (m), 806 (s), 792 (s), 739 (w), 717 (vs), 674 (vs), 600 (w), 526 (w), 499 (s), 475 (vs), 426 (m) cm^{-1}. The ^1H NMR spectrum of the [D$_6$]DMSO solution of **6** confirms the presence of *N*-methylpyridinium cations [signals at δ = 4.42 (s, 6 H, $CH_3NC_5H_5$), 8.03 (m, 4 H, $H^{3,5}$), 8.55 (t, J = 7.8 Hz, 2 H, H^4), and 8.92 (d, J = 5.9 Hz, 4 H, $H^{2,6}$) ppm].[20] Several sets of signals for pyrazine protons were observed, suggesting the presence of pyrazine in the free and coordinated states. Their integrals collectively amounted to 12 H.

$(PyH)_4[(Mo_2O_4Cl_4)_2(Pyz)_2]\cdot 2CH_3CN$ (7): $(PyH)_5[MoOCl_4(H_2O)]_3Cl_2$ (428 mg, 1.0 mmol of Mo) was dissolved in a mixture of acetonitrile (15 mL) and methanol (3 mL). Pyrazine (160 mg, 2.0 mmol) was added to this solution. A solution of a light green colour was left to stand in an evaporating dish under ambient conditions. Within 1 d, the colour of the concentrate changed to orange. Two phases were obtained after 4 d: orange crystals of **7** and large, brown crystals of **5**. The crystals of **7** became opaque when removed from the mother liquor. Dried sample: $C_{28}H_{32}Cl_8Mo_4N_8O_8$ (1276.0): calcd. C 26.36, H 2.53, N 8.78; found C 26.18, H 2.89, N 8.63. IR: $\tilde{\nu}$ = 2250 (w), 2089 (w), 1637 (w), 1612 (m), 1540 (m), 1411 (s), 1300 (m), 1253 (w), 1218 (w), 1200 (m), 1164 (s), 1122 (s), 1084 (w), 1052 (vs), 1020 (m), 1006 (m), 971 (vvs) and 953 (m, $\nu_{Mo=O}$), 873 (w), 807 (m), 788 (m), 753 (vvs), 716 (vvs), 679 (vs), 607 (s), 593 (s), 502 (s), 473 (vs), 417 (m) cm^{-1}.

$(PyH)_4[(Mo_2O_4Br_4)_2(Pyz)_2]\cdot 2CH_3CN$ (8): $\{(C_6H_5)_4P\}_2[(MoOBr_4)_2(Pyz)]\cdot 2CH_3CN$ (**4**) (170 mg, 0.10 mmol) was dissolved in a solution of methanol (1.0 mL) in acetonitrile (7.0 mL). Upon the addition of pyrazine (120 mg, 1.50 mmol), the solution immediately changed colour from orange to dark red. To this solution was added solid pyridinium bromide (120 mg, 0.75 mmol). A vial with

diethyl ether (5 mL) was carefully placed into the Erlenmeyer flask containing the reaction mixture. The flask was stoppered and left to stand under ambient conditions. A small amount of orange crystals of **8** deposited within 5 d. The crystals of **8** became opaque when removed from the mother liquor. Dried sample: $C_{28}H_{32}Br_8Mo_4N_8O_8$ (1631.6): calcd. C 20.61, H 1.98, N 6.87; found C 20.94, H 2.21, N 6.94. IR: $\tilde{\nu}$ = 2254 (w), 1637 (m), 1612 (m), 1539 (s), 1485 (vs), 1444 (w), 1411 (vs), 1390 (m), 1335 (m), 1308 (w), 1251 (w), 1220 (w), 1198 (m), 1163 (s), 1122 (s), 1082 (w), 1052 (vs), 1026 (w), 1019 (w), 1005 (w), 971 (vvs, $\nu_{Mo=O}$), 952 (m), 918 (sh.), 870 (w), 805 (m), 750 (vs), 720 (m), 704 (vvs), 679 (vs), 674 (vs), 607 (s), 594 (w), 490 (s), 473 (s), 416 (w) cm^{-1}.

X-ray Crystallography: The crystals used were mounted on the tip of glass fibres with a small amount of silicon grease and transferred to a goniometer head. Data were collected with a Nonius Kappa CCD diffractometer by using graphite monochromated Mo-K_α radiation. Data reduction and integration were performed with the software package DENZO-SMN.[42] Averaging of the symmetry-equivalent reflections largely compensated for the absorption effects. The coordinates of some or all of the non-hydrogen atoms were found via direct methods by using the structure solution program SHELXS.[43] The positions of the remaining non-hydrogen atoms were located by use of a combination of least-squares refinement and difference Fourier maps in the SHELXL-97 program.[43] With the exception of **2**, all non-hydrogen atoms were refined anisotropically. The asymmetric unit of **2** contained three $\{(C_2H_5)_4N\}^+$ cations: a whole cation residing on a general position and two halves which were both located with their nitrogen atoms on two-fold rotation axes in the *C*2/*c* space group. One of the latter was disordered. Its disorder was resolved by using PART –1 instruction. Even so, the displacement parameters of its atoms remained large. The hydrogen atoms were included in the structure factor calculations at idealized positions. All the calculations were performed using the WinGX program suite.[44] Figures depicting the structures were prepared by ORTEP3,[45] SHELXTL[46] and CrystalMaker.[47]

Table 4. Crystallographic data for **1**–**8**.

	1	**2**	**3**	**4**
Formula	$C_{28}H_{34}Cl_{10}Mo_2N_8O_2$	$C_{20}H_{44}Cl_8Mo_2N_4O_2$	$C_{56}H_{50}Cl_8Mo_2N_4O_2P_2$	$C_{56}H_{50}Br_8Mo_2N_4O_2P_2$
F_w	1061.01	848.07	1348.42	1704.10
Crystal system	triclinic	monoclinic	monoclinic	monoclinic
Space group	$P\bar{1}$	*C*2/*c*	$P2_1/n$	$P2_1/n$
T / K	150(2)	150(2)	150(2)	150(2)
a / Å	7.7024(2)	26.3833(3)	8.47880(10)	8.48450(10)
b / Å	10.8383(2)	15.7164(2)	14.5171(2)	14.6299(2)
c / Å	13.4129(3)	20.9304(2)	23.3941(3)	24.1094(3)
α / °	110.0754(13)	90	90	90
β / °	96.4529(14)	127.8393(6)	91.9014(8)	91.2103(7)
γ / °	92.0379(14)	90	90	90
V / Å^3	1041.72(4)	6853.94(13)	2877.94(6)	2991.97(7)
$\rho_{calcd.}$ / g cm^{-3}	1.691	1.644	1.556	1.892
Z	1	8	2	2
λ / Å	0.71073	0.71073	0.71073	0.71073
μ / mm^{-1}	1.281	1.380	0.908	5.858
Collected reflections	8586	15230	12568	12831
Unique reflections, R_{int}	4714, 0.0157	7829, 0.0166	6540, 0.0187	6784, 0.0293
Observed reflections	4314	7100	5644	5932
R_1[a] [$I > 2\sigma(I)$]	0.0250	0.0696	0.0267	0.0254
wR_2[b] [all data]	0.0627	0.2202	0.0701	0.0630
	5	**6**	**7**	**8**
Formula	$C_{18}H_{20}Cl_6Mo_2N_6O_3$	$C_{24}H_{30}Cl_8Mo_4N_8O_8$	$C_{32}H_{38}Cl_8Mo_4N_{10}O_8$	$C_{32}H_{38}Br_8Mo_4N_{10}O_8$
F_w	772.98	1225.92	1358.08	1713.76
Crystal system	monoclinic	monoclinic	triclinic	triclinic
Space group	$P2_1/n$	$P2_1/n$	$P\bar{1}$	$P\bar{1}$
T / K	150(2)	293(2)	150(2)	150(2)
a / Å	9.7328(2)	12.6178(3)	8.9679(2)	9.2119(1)
b / Å	12.1382(3)	13.2282(3)	12.1946(3)	12.4141(2)
c / Å	11.5645(2)	12.6889(3)	13.1469(3)	13.1960(2)
α / °	90	90	108.2292(14)	112.4664(9)
β / °	97.292(1)	116.4283(16)	105.3057(13)	97.059(1)
γ / °	90	90	107.2158(14)	107.934(1)
V / Å^3	1355.16(5)	1896.57(8)	1199.45(5)	1276.14(3)
$\rho_{calcd.}$ / g cm^{-3}	1.894	2.147	1.880	2.230
Z	2	2	1	1
λ / Å	0.71073	0.71073	0.71073	0.71073
μ / mm^{-1}	1.550	1.912	1.523	7.276
Collected reflections	5412	8451	9895	10653
Unique reflections, R_{int}	3084, 0.0114	4327, 0.0181	5442, 0.0184	5794. 0.0199
Observed reflections	2852	3342	4938	5303
R_1[a] [$I > 2\sigma(I)$]	0.0197	0.0353	0.0257	0.0236
wR_2[b] [all data]	0.0485	0.0944	0.0639	0.0586

[a] $R_1 = \Sigma||F_o| - |F_c||/\Sigma|F_o|$. [b] $wR_2 = \{\Sigma[w(F_o^2 - F_c^2)^2]/\Sigma[w(F_o^2)^2]\}^{1/2}$.

Cell parameters and refinement results are summarized in Table 4. CCDC-742197 (for **1**), -742198 (for **2**), -742199 (for **3**), -742200 (for **4**), -742201 (for **5**), -742202 (for **6**), -742203 (for **7**) and -742204 (for **8**) contain the supplementary crystallographic data for this paper. These data can be obtained free of charge from The Cambridge Crystallographic Data Centre via www.ccdc.cam.ac.uk/data_request/cif.

Supporting Information (see footnote on the first page of this article): ORTEP drawings of **4** and **8**; drawings of the hydrogen-bonding pattern and π–π-type interactions in **6**; listings of relevant bond lengths and angles for compounds **1**–**8**; TGA profiles for **3** and **4**.

Acknowledgments

We thank Prof. Darko Dolenc for recording the NMR spectra and Prof. Boris Pihlar for helpful suggestions with the electrochemical experiments. The work was supported by the Slovenian Ministry of Higher Education, Science and Technology through the research grant P1-0134. R.C. thanks The European Network of Excellence: "Molecular Approach to Nanomagnets and Multifunctional Materials" (MAGMANet, NMP3-CT-2005-515767), the "Région Aquitaine", University of Bordeaux and the Centre National de la Recherche Scientifique (CNRS) for financial support.

[1] a) E. I. Stiefel, *Prog. Inorg. Chem.* **1977**, *22*, 1–223; b) F. A. Cotton, *J. Less-Common Met.* **1974**, *36*, 13–22.
[2] a) A. B. Blake, F. A. Cotton, J. S. Wood, *J. Am. Chem. Soc.* **1964**, *86*, 3024–3031; b) F. A. Cotton, S. M. Morehouse, *Inorg. Chem.* **1965**, *4*, 1377–1381; c) P. C. H. Mitchell, *Q. Rev., Chem. Soc.* **1966**, *20*, 103–118.
[3] Complexes with the *anti*-$\{Mo_2O_4\}^{2+}$ core are very rare. See for example: K. Wieghardt, M. Hahn, W. Swiridoff, J. Weiss, *Angew. Chem. Int. Ed. Engl.* **1983**, *22*, 491–492.
[4] J. Bernholc, N. A. W. Holzwarth, *J. Chem. Phys.* **1984**, *81*, 3987–3995.
[5] a) T. Chandler, D. L. Lichtenberger, J. H. Enemark, *Inorg. Chem.* **1981**, *20*, 75–77; b) P. Rabe, J. E. Guerchais, J. Sala Pala, M. El Khalifa, J.-Y. Saillard, L. Toupet, *Polyhedron* **1993**, *12*, 1215–1225.
[6] Unless stated otherwise, by the $\{Mo_2O_4\}^{2+}$ structural unit we refer to the more common *syn* isomer.
[7] a) H. K. Chae, W. G. Klemperer, T. A. Marquart, *Coord. Chem. Rev.* **1993**, *128*, 209–224; b) B. Modec, J. V. Brenčič, *J. Cluster Sci.* **2002**, *13*, 279–302.
[8] a) F. A. Cotton, L. M. Daniels, C. Lin, C. A. Murillo, *Chem. Commun.* **1999**, 841–842; b) F. A. Cotton, L. M. Daniels, C. Lin, C. A. Murillo, *J. Am. Chem. Soc.* **1999**, *121*, 4538–4539; c) F. A. Cotton, C. Lin, C. A. Murillo, *Acc. Chem. Res.* **2001**, *34*, 759–771; d) F. A. Cotton, J. P. Donahue, C. A. Murillo, *J. Am. Chem. Soc.* **2003**, *125*, 5436–5450; e) M. H. Chisholm, A. M. Macintosh, *Chem. Rev.* **2005**, *105*, 2949–2976; f) J. P. Donahue, C. A. Murillo, *Dalton Trans.* **2008**, 1547–1551.
[9] a) M. H. Chisholm, K. Folting, J. C. Huffman, C. C. Kirkpatrick, *Inorg. Chem.* **1984**, *23*, 1021–1037; b) S. Lincoln, S. A. Koch, *Inorg. Chem.* **1986**, *25*, 1594–1602; c) B. Modec, D. Dolenc, J. V. Brenčič, *Inorg. Chim. Acta* **2007**, *360*, 663–678.
[10] a) M. F. Belicchi, G. G. Fava, C. Pelizzi, *J. Chem. Soc., Dalton Trans.* **1983**, 65–69; b) H. Kang, S. Liu, S. N. Shaikh, T. Nicholson, J. Zubieta, *Inorg. Chem.* **1989**, *28*, 920–933; c) B. Modec, J. V. Brenčič, J. Zubieta, *J. Chem. Soc., Dalton Trans.* **2002**, 1500–1507; d) M. D. Meienberger, B. Morgenstern, S. Stucky, K. Hegetschweiler, *Eur. J. Inorg. Chem.* **2008**, 129–137.
[11] a) R. Mattes, K. Mühlsiepen, *Z. Naturforsch., Teil B* **1980**, *35*, 265–268; b) W. Schirmer, U. Flörke, H. J. Haupt, *Z. Anorg. Allg. Chem.* **1989**, *574*, 239–255; c) G. S. Kim, D. A. Keszler, C. W. DeKock, *Inorg. Chem.* **1991**, *30*, 574–577; d) B. Modec, J. V. Brenčič, E. M. Burkholder, J. Zubieta, *Dalton Trans.* **2003**, 4618–4625.
[12] B. Modec, J. V. Brenčič, *Eur. J. Inorg. Chem.* **2005**, 4325–4334.
[13] B. Modec, J. V. Brenčič, J. Koller, *Eur. J. Inorg. Chem.* **2004**, 1611–1620.
[14] a) M. J. Manos, A. D. Keramidas, J. D. Woollins, A. M. Z. Slawin, T. A. Kabanos, *J. Chem. Soc., Dalton Trans.* **2001**, 3419–3420; b) E. Dumas, C. Sassoye, K. D. Smith, S. C. Sevov, *Inorg. Chem.* **2002**, *41*, 4029–4032; c) C. du Peloux, A. Dolbecq, P. Mialane, J. Marrot, F. Secheresse, *Dalton Trans.* **2004**, 1259–1263; d) M. J. Manos, J. D. Woollins, A. M. Z. Slawin, T. A. Kabanos, *Angew. Chem. Int. Ed.* **2002**, *41*, 2801–2805; e) D. Liu, P. Zhang, J. Xu, S. Feng, Z. Shi, *Solid State Sci.* **2007**, *9*, 16–20; f) M.-Y. Lee, S.-L. Wang, *Chem. Mater.* **1999**, *11*, 3588–3594.
[15] M. K. Ehlert, S. J. Rettig, A. Storr, R. C. Thompson, J. Trotter, *Inorg. Chem.* **1993**, *32*, 5176–5182.
[16] Selected examples from recent literature include dinuclear species: a) M. Willermann, C. Mulcahy, R. K. O. Sigel, M. M. Cerda, E. Freisinger, P. J. S. Miguel, M. Roitzsch, B. Lippert, *Inorg. Chem.* **2006**, *45*, 2093–2099; b) D. Matoga, J. Szklarzewicz, J. Fawcett, *Polyhedron* **2005**, *24*, 1533–1539; trinuclear species: c) X.-Y. Yu, M. Maekawa, M. Kondo, S. Kitagawa, G.-X. Jin, *Chem. Lett.* **2001**, 168–169; d) M. Schweiger, S. R. Seidel, A. M. Arif, P. J. Stang, *Angew. Chem. Int. Ed.* **2001**, *40*, 3467–3469; tetranuclear species: e) J. K. Clegg, L. F. Lindoy, J. C. McMurtrie, D. Schilter, *Dalton Trans.* **2005**, 857–864; f) B. Manimaran, T. Rajendran, Y.-L. Lu, G.-H. Lee, S.-M. Peng, K.-L. Lu, *J. Chem. Soc., Dalton Trans.* **2001**, 515–517; g) T. Fujimura, H. Seino, M. Hidai, Y. Mizobe, *Inorg. Chim. Acta* **2005**, *358*, 2449–2453; h) P. H. Dinolfo, M. E. Williams, C. L. Stern, J. T. Hupp, *J. Am. Chem. Soc.* **2004**, *126*, 12989–13001; polymeric species: i) S. Takamizawa, E. Nakata, T. Saito, T. Akatsuka, *Inorg. Chem.* **2005**, *44*, 1362–1366; j) S. A. Barnett, A. J. Blake, N. R. Champness, C. Wilson, *Dalton Trans.* **2005**, 3852–3861.
[17] Our previous work has shown that the addition of weak bases such as pyridine or carboxylate ions to an acetonitrile solution of $(PyH)_5[MoOCl_4(H_2O)]_3Cl_2$ caused an immediate change in colour to deep orange due to the formation of $\{Mo_2O_4\}^{2+}$ species: B. Modec, J. V. Brenčič, *Eur. J. Inorg. Chem.* **2005**, 1698–1709.
[18] $2(PyH)_5[MoOCl_4(H_2O)]_3Cl_2 + 3Pyz + 2PyHCl + 6CH_3CN \rightarrow 3(PyH)_4[(MoOCl_4)_2(Pyz)]Cl_2{\cdot}2CH_3CN + 6H_2O$. The addition of an excess amount of pyridinium chloride (115 mg, 1.0 mmol) to the reaction mixture, described for the preparation of **1**, leads to a better yield. On average, 420 mg of **1** was isolated. Yield: 79%.
[19] Such a sequence of reactions was demonstrated by the transformation of $[Mo_2O_3(OMe)(OOCCH_3)Cl_4]^{2-}$, a complex with a bridging methoxide, into the $\{Mo_2O_4\}^{2+}$-containing products: B. Modec, *Inorg. Chem. Commun.* **2009**, *12*, 328–331.
[20] D. Dolenc, B. Modec, *Acta Chim. Slov.* **2008**, *55*, 752–756.
[21] S. Parsons, X. Liu, L. Yellowlees, P. Wood, Private communication to the Cambridge Structural Database, **2004**. Deposition number CCDC-247870.
[22] The two earliest examples, $MoOCl_3{\cdot}Pyz$ and $MoOCl_3{\cdot}2Pyz$ [W. M. Carmichael, D. A. Edwards, *J. Inorg. Nucl. Chem.* **1970**, *32*, 1199–1207], are not included in Table 2. The lack of X-ray structural data precludes unambiguous conclusions about the true identity of either of the two compounds.
[23] D. Matoga, J. Szklarzewicz, A. Samotus, K. Lewinski, *J. Chem. Soc., Dalton Trans.* **2002**, 3587–3592.
[24] Y. Liang, M. Hong, R. Cao, D. Sun, J. Weng, *Acta Crystallogr., Sect. E* **2001**, *57*, m159–m161.
[25] a) M. M. El-Essawi, F. Weller, K. Stahl, M. Kersting, K. Dehnicke, *Z. Anorg. Allg. Chem.* **1986**, *542*, 175–181; b) A. A. Eagle, M. F. Mackay, C. G. Young, *Inorg. Chem.* **1991**, *30*, 1425–1428; c) L.-Z. Cai, L.-J. Song, H.-Y. Zeng, Z.-C. Dong, G.-C. Guo, J.-S. Huang, *Inorg. Chim. Acta* **2003**, *344*, 61–64.

[26] The sum of the corresponding van der Waals radii is 3.10 Å. Data were taken from B. Douglas, D. McDaniel, J. Alexander, *Concepts and Models of Inorganic Chemistry*, 3rd ed., Wiley, New York, **1994**, p. 102.

[27] B. Modec, D. Dolenc, M. Kasunič, *Inorg. Chem.* **2008**, *47*, 3625–3633.

[28] The distance between the centroids is given.

[29] C. Janiak, *J. Chem. Soc., Dalton Trans.* **2000**, 3885–3896.

[30] B. Bleaney, K. D. Bowers, *Proc. R. Soc. London, Ser. A* **1952**, *214*, 451–465.

[31] A 2.0 mM solution of $\{(C_2H_5)_4N\}[MoOX_4(H_2O)]$ (X = Cl, Br) was used. The mononuclear complexes were prepared from $[Mo_2(OOCCH_3)_4]$ following a published procedure (A. Bino, F. A. Cotton, *Inorg. Chem.* **1979**, *18*, 2710–2713).

[32] This is supported with the CV of DMF, to which a small amount of hydrochloric acid was added, which also revealed a strong reduction wave at this potential.

[33] UV/Vis of DMF solution of $\{(C_2H_5)_4N\}[MoOCl_4(H_2O)]$: λ (ε / $L\,mol^{-1}\,cm^{-1}$) = 365 (sh., 350), 455 (20), 745 (15) nm.

[34] The UV/Vis data for **2**, **3** and **4**, listed in the Experimental part, pertain to the species present in solution.

[35] a) J. A. Craig, E. W. Harlan, B. S. Snyder, M. A. Whitener, R. H. Holm, *Inorg. Chem.* **1989**, *28*, 2082–2091; b) S. A. Roberts, C. G. Young, C. A. Kipke, W. E. Cleland Jr., K. Yamanouchi, M. D. Carducci, J. H. Enemark, *Inorg. Chem.* **1990**, *29*, 3650–3656.

[36] The choice of DMF as a solvent was necessitated by the low solubility of **5** in other solvents.

[37] a) W. E. Newton, J. L. Corbin, D. C. Bravard, J. E. Searles, J. W. McDonald, *Inorg. Chem.* **1974**, *13*, 1100–1104; b) L. J. De Hayes, H. C. Faulkner, W. H. Doub, D. T. Sawyer, *Inorg. Chem.* **1975**, *14*, 2110–2116; c) T. Matsuda, K. Tanaka, T. Tanaka, *Inorg. Chem.* **1979**, *18*, 454–457; d) K. F. Miller, R. A. D. Wentworth, *Inorg. Chem.* **1980**, *19*, 1818–1821.

[38] C. G. Barraclough, J. Lewis, R. S. Nyholm, *J. Chem. Soc.* **1959**, 3552–3555.

[39] a) W. E. Newton, J. W. McDonald, *J. Less-Common Met.* **1977**, *54*, 51–62; b) S. E. Lincoln, T. M. Loehr, *Inorg. Chem.* **1990**, *29*, 1907–1915; c) Z. Xiao, J. H. Enemark, A. G. Wedd, C. G. Young, *Inorg. Chem.* **1994**, *33*, 3438–3441; d) K. R. Barnard, M. Bruck, S. Huber, C. Grittini, J. H. Enemark, R. W. Gable, A. G. Wedd, *Inorg. Chem.* **1997**, *36*, 637–649.

[40] N. B. Colthup, L. H. Daly, S. E. Wiberley, *Introduction to Infrared and Raman Spectroscopy*, Academic Press, **1964**, p. 202.

[41] F. A. Cotton, D. M. L. Goodgame, M. Goodgame, A. Sacco, *J. Am. Chem. Soc.* **1961**, *83*, 4157–4161.

[42] Z. Otwinowski, W. Minor, *Methods Enzymol.* **1997**, *276*, 307–326.

[43] G. M. Sheldrick, *SHELXS-97* and *SHELXL-97*, University of Göttingen, **1997**.

[44] *WinGX*: L. J. Farrugia, *J. Appl. Crystallogr.* **1999**, *32*, 837–838.

[45] *ORTEP3* for Windows: L. J. Farrugia, *J. Appl. Crystallogr.* **1997**, *30*, 565.

[46] *SHELXTL*, version 5.03, Siemens Analytical X-ray Instrument Division, Madison, WI, **1994**.

[47] *CrystalMaker for Windows*, version 2.15, CrystalMaker Software Ltd., Oxfordshire, UK, **2008**.

Received: August 3, 2009
Published Online: December 22, 2009

